# Probing past mergers of supermassive black holes with pulsar timing arrays: The role of pulsar terms

Hippolyte Quelquejay Leclere*

*Dipartimento di Fisica "G. Occhialini," Università degli Studi di Milano-Bicocca, Piazza della Scienza 3, I-20126 Milan, Italy*

(Received 13 March 2026; accepted 30 July 2026; published 24 August 2026)

By monitoring the times of arrival of radio pulses from millisecond pulsars, pulsar timing arrays (PTAs) serve as unique gravitational wave (GW) laboratories in the nanohertz band. To date, the primary astrophysical sources of GWs targeted in this frequency range have been inspiraling supermassive black hole binaries (SMBHBs) on circular and eccentric orbits. In this work, we demonstrate that, thanks to the so-called pulsar term in the timing residual waveform of GW signals, PTAs can probe individual SMBHBs that merged before timing observations began. We refer to the latter as *zombie binaries*. Using SMBHB population models consistent with current PTA constraints, we find that while the probability of detecting such systems in existing PTA datasets remains low, the Square Kilometer Array observatory is expected to achieve sufficient sensitivity to have a few zombie binaries with optimal matched filter signal-to-noise ratios exceeding 3 in its data. Although their confident identification might be challenging, this new class of PTA sources opens a novel window for studying the most massive SMBHBs in our local universe.

DOI: 10.1103/9wq2-gqkh

## I. INTRODUCTION

Recently, pulsar timing array (PTA) Collaborations have reported compelling evidence for the presence of gravitational wave (GW) signals in their datasets [1–5]. The primary source of these nanohertz GWs is believed to be the population of inspiraling supermassive black hole binaries (SMBHBs) [6,7], which are expected to form within the hierarchical model of galaxy formation [8,9]. If supermassive black hole pairs manage to efficiently reach subparsec separation within a Hubble time [10]—through dynamical friction and stellar hardening [11,12]—they become efficient sources of GWs in the 1–100 nanohertz band, until they merge at orbital frequencies of hundreds of nanohertz. Therefore, binaries emitting in the PTA band are generally thousands to millions of years from merger and are thus expected to be observed as quasimonochromatic sources over PTAs timescale.

Up to now, PTAs have searched for SMBHBs using three main approaches. The first involves detecting the stochastic GW background produced by the population of binaries, which is expected to imprint a quadrupolar correlation pattern among pulsars' timing residuals, known as the Hellings-Downs curve [13]. The presence of such a signal has been reported with strong evidence by various PTAs, along with a characterization of its power spectral density in the 1–10 nanohertz range, mostly consistent across Collaborations [14]. Although potentially degenerate with, for example, other cosmological GW backgrounds [15,16], the identification of significant anisotropies [17,18], nonstationarities [19] or non-Gaussianities [20,21] could help proving the astrophysical origin of the stochastic signal. But collaborations have not yet found strong evidence of such features [22–25].

The second, more direct approach is the search for GW signals from individual binaries, inspiraling on circular or eccentric orbits, in the PTA data [26–28]. The pulsars' timing residuals induced by an inspiraling SMBHB are made of two terms, respectively produced by the metric perturbation at the pulse emissions (pulsar term) and their reception (Earth term). Assuming that the SMBHB dynamics is driven by GWs emission, a deterministic template for both the Earth and pulsar terms in each pulsar timing residuals can be derived and searched for in PTA data. So far, no conclusive evidence for the presence of such a system has been reported [29,30].

Finally, PTAs are also sensitive to the GW memory signal produced by SMBHB coalescences. If the memory wavefront from a binary merger passes through the Earth during the detector's observation period, it will—at leading order—produce deterministic linear trends in the pulsars' timing residuals (see Refs. [31–34] for further discussion of memory signals in PTA data). While in principle

*Contact author: hippolyte.quelquejayleclere@unimib.it

*Published by the American Physical Society under the terms of the Creative Commons Attribution 4.0 International license. Further distribution of this work must maintain attribution to the author(s) and the published article's title, journal citation, and DOI.*

observable, these events are expected to be rare, as they require a sufficiently massive and nearby SMBHB to merge during the PTA observing campaign. Nonetheless, searches for memory burst signatures in PTA data have been carried out and have yielded constraints on the merger rate of SMBHBs in our local Universe [35,36].

Pitkin [37] was the first to notice that the signal from an individual SMBHB could take a distinct form in the case of a SMBHB merging in the millihertz band of the Laser Interferometer Space Antenna (LISA) detector. In this scenario, the Earth terms associated with this binary would be at a too high frequency to be probed by PTAs, but the pulsar terms could still fall within their sensitivity band, thereby enabling the possibility of multiband observations of SMBHBs [38]. In this work, we extend beyond the case of binaries merging at present and show that PTAs are also sensitive to past mergers of SMBHB, due to the kiloparsec-scale distances between the monitored pulsars and Earth. Hereafter, we refer to this new class of PTA sources as *zombie binaries*. The paper is organized as follows. In Sec. II, we first explain the principles of zombie binary detection with PTAs. We then estimate the likelihood of observing zombie binaries with high signal-to-noise ratio (SNR) in PTA datasets in Sec. III. This depends both on the SMBHB population models considered, which we present in Sec. IV, and on the PTA sensitivity to zombie binary signals, which we estimate in Sec. V. We then present our results for past, current, and future PTA sensitivities in Sec. VI, before discussing the implications of our findings in Sec. VII.

In the following, $G$ is Newton's gravitational constant, $c$ is the speed of light in vacuum and log denotes the base 10 logarithm.

## II. ZOMBIE BINARY SIGNALS

In PTAs, the signal produced by a GW source consists of two contributions, usually referred to in the literature as the Earth term and the pulsar term [39]. The arrival time of a radio pulse emitted by a pulsar $a$ is influenced by the metric perturbation both at the moment of its emission (at the pulsar) and at the moment of its reception (at Earth). This is explicit in the expression of the induced timing residuals (see e.g., Ref. [40]),

$$R^{(a)}_{\rm GW}(t) = \sum_{A\in\{+,\times\}} F^A_a \int^t \mathrm{d}t' [h_A(t') - h_A(t'-\tau_a)], \quad (1)$$

where $h_A$ denotes the plane-wave metric perturbation propagating along $\hat{n}$, and $F^A_a$ are the antenna pattern response functions of the pulsar for the $+$ and $\times$ polarization modes which, using Einstein summation on spatial indices $i$, $j$, can be expressed as

$$F^A_a \equiv \frac{\hat{p}^i_a \hat{p}^j_a e^A_{ij}(\hat{n})}{2(1+\hat{n}\cdot\hat{p}_a)}. \quad (2)$$

We introduced the polarization tensors $e^A$ and the unit position vector of pulsar $a$, $\hat{p}_a$.

In Eq. (1), we see that while the Earth term of the timing residuals correspond to the integrated strain signal today, the pulsar term introduces a geometrical time delay,

$$\tau_a \equiv (1+\hat{p}_a\cdot\hat{n})T_a, \quad (3)$$

where $T_a \equiv D_a/c$ is the unperturbed time of flight to Earth of the radio photons[1] emitted by pulsar $a$. For Galactic pulsars monitored by PTAs, the corresponding time delay is on the order of several thousand years and attains its maximum value of $2T_a$ when the GW source lies in the direction on the sky opposite to that of the pulsar.

In this work, we investigate the possibility to probe binaries that either merged before the PTA experiment began or which are on the verge of merging. For such systems, the corresponding Earth terms vanish or lie outside the PTA band. However, some pulsars can still exhibit nonzero pulsar terms for binaries that coalesced on timescales up to thousands of years in the past. We therefore refer to this new class of PTA sources as *zombie binaries*.

At 0 post-Newtonian (PN) order, the orbital frequency evolution of SMBHBs on circular orbit with dynamics driven by GW emission is, in the observer frame, given by [41]

$$\frac{\mathrm{d}f_{\rm orb}}{\mathrm{d}t} = \frac{1}{2\pi}\frac{96}{5}\left(\frac{G\mathcal{M}_{\rm c}}{c^3}\right)^{5/3}(2\pi f_{\rm orb})^{11/3}, \quad (4)$$

where $\mathcal{M}_{\rm c} = M_1^{3/5}M_2^{3/5}/(M_1+M_2)^{1/5}$ is the observer-frame binary chirp mass. Because Eq. (4) strongly depends on the binary's orbital frequency, $f_{\rm orb}$, a zombie binary that merged before the start of the PTA experiment could still produce pulsar term signals within the PTA frequency band. Indeed, for a binary that coalesced at time $t_{\rm c}$ in the observer frame, the orbital frequency of the binary as seen in the pulsar term of a given pulsar can be obtained by integrating Eq. (4), assuming that at $t_{\rm c}$, we have $f_{\rm orb} = f^{(\rm ISCO)}_{\rm orb}$, the orbital frequency of the binary at its innermost stable circular orbit. This yields,

$$f^{(\rm P,a)}_{\rm orb} = f^{(\rm ISCO)}_{\rm orb}\left[1+\frac{\tau_a-\tau_{\rm c}}{T_{\rm c}(f^{(\rm ISCO)}_{\rm orb})}\right]^{-3/8}, \quad (5)$$

where $\tau_{\rm c} \equiv t_0 - t_{\rm c}$, is the time delay separating the starting date of the PTA observations, $t_0$, from the binary merger.

[1]In this study, we do not consider any chromatic effect on the timing residuals and assume that all observations are done at a radio frequency of 1400 MHz.

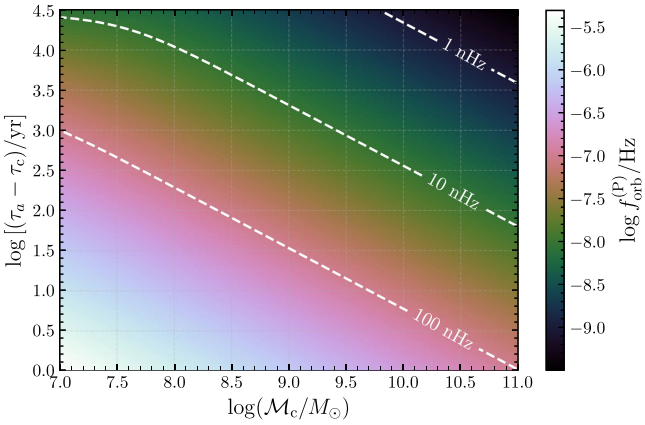



FIG. 1. Initial orbital frequency of the binary in the pulsar term signal, expressed as a function of the observer-frame binary chirp mass and the time delay separating the pulsar term epoch from the binary merger, $\tau_a - \tau_c$. We assume here that the binary mass ratio is 1.

We introduced the characteristic coalescence time of the binary from the orbital frequency $f_{\mathrm{orb}}$, $T_c(f_{\mathrm{orb}}) \equiv 5/256(G\mathcal{M}_c/c^3)^{-5/3}(2\pi f_{\mathrm{orb}})^{-8/3}$. We emphasize that we assume the binaries have been on circular orbits for the last few thousand years preceding their merger, with dynamics driven solely by GW emission. We therefore only consider the binaries GW radiation at $2f_{\mathrm{orb}}$ [42]. The effect of eccentricity, interaction with the binary disks as well as the impact of higher-order PN dynamics will be explored in future work.

Figure 1 illustrates how the zombie binary's orbital frequency—as observed in the pulsar term—varies with both the binary chirp mass and the time delay separating the pulsar term epoch from the binary merger. We see that for binaries with $\mathcal{M}_c \geq 10^9 M_\odot$, time delays of thousands of years are sufficient for the binary to have GW frequency well within the PTA band, around 10 nanohertz. Therefore, zombie binaries that merged thousands of years before the start of any PTA experiment could be observable in PTA datasets as quasimonochromatic sine waves whose frequency and amplitude are specific to each pulsar depending on their relative position to the binary and their distance from Earth. However, a zombie binary will affect the timing residuals of a given pulsar $a$ only if $\tau_a > \tau_c$. Otherwise, the pulsar term epochs observed by pulsar $a$ would correspond to the postmerger phase of the binary's evolution, and thus will not be associated with any GW signal. Therefore, the further back in time the merger occurred, the less likely it is that pulsars in the PTA will contribute to its detection.

## III. OCCURRENCE OF ZOMBIE BINARIES

We now aim to quantify the probability of having resolvable zombie binaries in a given PTA dataset. To assess the detectability of a zombie binary, we use the system's optimal matched filter SNR and rely on specific SNR thresholds to estimate its detectability.

In the following, we define zombie binaries as binaries whose Earth term orbital frequency at $t_0$, $f_{\mathrm{orb}}^{(\mathrm{E})}$, exceeds a threshold frequency, $f_{\mathrm{th}}$. We note that this includes the case of binaries that merged before $t_0$, for which we consider that $f_{\mathrm{orb}}^{(\mathrm{E})} = +\infty$. In this paper, we use $f_{\mathrm{th}} = 3 \times 10^{-7}$ Hz $\approx 1/(2 \times 19$ days), a frequency at the edge of the PTA band. We emphasize that increasing this threshold has a negligible impact on our results, since the number of binaries that merge during the PTA observation (or shortly thereafter) is negligible compared to the number of binaries that have merged in the past thousands of years.

Since zombie binaries may already have coalesced at $t_0$, instead of distributing the SMBHBs over their Earth term orbital frequency—as is usually done in the PTA literature [43–45]—we use their coalescence time as dynamical variable, through $\tau_c$. The distribution of merging SMBHBs can be obtained from their comoving merger density, $n$, using

$$\frac{\mathrm{d}^4 N}{\mathrm{d}\vec{\xi}_{\mathrm{I}}\mathrm{d}\tau_c} = \frac{\mathrm{d}^3 n}{\mathrm{d}\vec{\xi}_{\mathrm{I}}}\frac{\mathrm{d}z}{\mathrm{d}\tau_{c,r}}\frac{\mathrm{d}V_c}{\mathrm{d}z}\frac{\mathrm{d}\tau_{c,r}}{\mathrm{d}\tau_c} \tag{6}$$

$$= \frac{\mathrm{d}^3 n}{\mathrm{d}\vec{\xi}_{\mathrm{I}}}\frac{4\pi c d_L^2}{(1+z)^2}, \tag{7}$$

where we distribute the binaries over redshift, rest-frame chirp mass (expressed in base-10 logarithm of solar masses), and mass ratio, using the vector $\vec{\xi}_{\mathrm{I}} = (z, \log \mathcal{M}_{c,r}, q)$. In Eq. (7), $d_L$ denotes the luminosity distance to a binary at redshift $z$—computed using the Planck 2018 cosmology [46]—which enters the expression for the differential comoving volume element, $\mathrm{d}V_c/\mathrm{d}z$ [47]. Note that quantities evaluated in the binary rest frame are systematically indexed by the subscript r.

Given our definition of zombie binaries, we can compute their average number across universe realizations by integrating Eq. (7) over the corresponding $\tau_c$ range. The first condition that a zombie binary must meet is that $f_{\mathrm{orb}}^{(\mathrm{E})} \geq f_{\mathrm{th}}$, since their associated Earth terms must be null or inaccessible to PTAs. Using Eq. (5) with $\tau_a = 0$, this reads

$$\tau_c \geq \tau_c^{(\mathrm{min})} \equiv T_c(f_{\mathrm{orb}}^{(\mathrm{ISCO})})\left[1 - \left(\frac{f_{\mathrm{th}}}{f_{\mathrm{orb}}^{(\mathrm{ISCO})}}\right)^{-8/3}\right]. \tag{8}$$

We note that, for highly massive binaries satisfying $f_{\mathrm{orb}}^{(\mathrm{ISCO})} \leq f_{\mathrm{th}}$, this condition is replaced by $\tau_c \geq 0$, to ensure that the binary merges before $t_0$. In addition, a zombie binary can potentially be detected by a PTA only if its inspiral can be observed at least by the pulsar term of the most distant pulsar of the array. A zombie binary therefore

must also verify $\tau_c \leq 2T^{(\max)}$, where $T^{(\max)}$ is the photons' time of flight associated with this most distant pulsar.

Consequently, the average number of zombie binary signals potentially present in a given PTA dataset can be evaluated using

$$\langle N \rangle = \int \mathrm{d}\vec{\xi}_I \frac{\mathrm{d}^3 n}{\mathrm{d}\vec{\xi}_I} \frac{4\pi c d_L^2}{(1+z)^2} (2T^{(\max)} - \tau_c^{(\min)}), \quad (9)$$

where we omitted the dependence of $\tau_c^{(\min)}$ over $\vec{\xi}_I$. Since a large fraction of these zombie binaries will correspond to very low SNR values regardless of the PTA considered, we instead compute the expectation value for the number of zombie binaries with a SNR higher than a certain threshold $\mathrm{SNR}_{\mathrm{th}}$,

$$\langle N_z \rangle \equiv \int \mathrm{d}\vec{\xi}_I \frac{\mathrm{d}^3 n}{\mathrm{d}\vec{\xi}_I} \frac{4\pi c d_L^2}{(1+z)^2} (2T^{(\max)} - \tau_c^{(\min)}) \times \mathrm{P}(\mathrm{SNR} \geq \mathrm{SNR}_{\mathrm{th}} | \vec{\xi}_I), \quad (10)$$

introducing the detection efficiency of the PTA, $\mathrm{P}(\mathrm{SNR} \geq \mathrm{SNR}_{\mathrm{th}} | \vec{\xi}_I)$. This function gives the probability that a zombie binary with intrinsic parameters, $\vec{\xi}_I$, yields a SNR above $\mathrm{SNR}_{\mathrm{th}}$ for a given PTA configuration.

In the following, we consider $\mathrm{SNR}_{\mathrm{th}} \in \{3, 5, 10\}$. In principle, the SNR threshold should be calibrated from the distribution of the detection statistic under the null hypothesis (i.e., noise-only datasets) for a prescribed false alarm probability [48]. However, estimating this distribution raises several methodological challenges that are beyond the scope of this study and will be addressed in future work. We therefore consider a range of SNR thresholds in order to assess the robustness of our results with respect to the threshold choice.

The 3D integral of Eq. (10) can be accurately approximated by the 2D integral over binary redshift and chirp mass. Indeed, it is straightforward to verify that for the range of binary intrinsic parameters considered in this study,[2] $2T^{(\max)} - \tau_c^{(\min)} \approx 2T^{(\max)}$. Furthermore, for comparable mass binaries, under the assumption of GW-driven dynamics at 0 PN order, the binary mass ratio only enters in the zombies waveforms via $f_{\mathrm{orb}}^{(\mathrm{ISCO})}$ and thus have only a negligible effect on the detection efficiency. We can therefore neglect the dependence over the binary mass ratio in Eq. (10). For the remaining parameters, we consider $z \in [10^{-2}, 4]$ and $\log \mathcal{M}_{c,r}/M_\odot \in [7.5, 11]$.

[2]We note that for binaries with $\mathcal{M}_c \ll 10^8 M_\odot$, this approximation no longer holds. However, such low-mass systems are associated with a zero detection efficiency for the PTAs considered in this work. Therefore, the region of the zombie parameter space with $\mathcal{M}_{c,r} < 10^8 M_\odot$ does not contribute to the evaluation of Eq. (10).

Since incorporating the PTA detection efficiency in Eq. (10) is equivalent to thinning the Poisson process [49] governing the occurrence of merging SMBHBs, the number of zombie binaries yielding a SNR above $\mathrm{SNR}_{\mathrm{th}}$ follows a Poisson distribution of mean $\langle N_z \rangle$. Once the latter is computed for a given comoving merger density model and a given PTA sensitivity, the probability to have at least one zombie binary with $\mathrm{SNR} \geq \mathrm{SNR}_{\mathrm{th}}$ can be obtained using $\mathrm{P}(N_z > 0) = 1 - e^{-\langle N_z \rangle}$.

## IV. COMOVING MERGER DENSITY MODELS

In order to compute Eq. (10), one needs a model for the comoving SMBHB merger density function, $n$. We model it using the Schechter-like parametric model introduced in [50],

$$\frac{\mathrm{d}^2 n}{\mathrm{d}z \mathrm{d}\log \mathcal{M}_{c,r}} = \dot{n}_0 \left[ \left( \frac{\mathcal{M}_{c,r}}{10^7 M_\odot} \right)^{-\alpha} e^{-\mathcal{M}_{c,r}/\mathcal{M}_{c,\star}} \right] \times [(1+z)^\beta e^{-z/z_0}] \frac{\mathrm{d}t_r}{\mathrm{d}z}, \quad (11)$$

which depends on five parameters; the spectral indices $\alpha$ and $\beta$, the chirp mass and redshift exponential cutoffs $\mathcal{M}_{c,\star}$ and $z_0$ and the comoving merger rate normalizing factor, $\dot{n}_0$.

In order to quantify the dependence of our results on the comoving merger density model, we follow [51] and consider three different sets of parameters, given in Table I. For each model, we adjust the value of $\dot{n}_0$ so that the GW background characteristic strain amplitude induced by the population is consistent with current PTA observations. Using the Phinney theorem [52], we set $h_c(f = 1/\mathrm{year}) = 3 \times 10^{-15}$.

The comoving merger density associated with each model—integrated over redshift—are shown in Fig. 2. We note that our choice of models reflects the current uncertainty regarding the population of SMBHBs likely to be responsible for the PTA signal [16,53]. For example, M1 includes a large number of relatively low-mass binaries, while M2 favors a smaller number of higher-mass systems.

## V. THE ZOMBIE DETECTION EFFICIENCY

The second ingredient needed to evaluate $\langle N_z \rangle$ is the detection efficiency which only depends on the PTA configuration considered. Since here, we neglect the influence of

TABLE I. Parameters used for the three comoving merger density models employed in this work.

| Name | $\alpha$ | $\log \mathcal{M}_{c,\star}/M_\odot$ | $\beta$ | $z_0$ | $\dot{n}_0$ [$\mathrm{Gyr}^{-1}\mathrm{Mpc}^{-3}$] |
|---|---|---|---|---|---|
| M1 | −0.5 | 8.5 | 1.5 | 1.1 | $1.83 \times 10^{-4}$ |
| M2 | −1 | 9 | 1 | 0.5 | $2.25 \times 10^{-6}$ |
| M3 | 0.5 | 9.3 | 0.5 | 1 | $1.26 \times 10^{-3}$ |

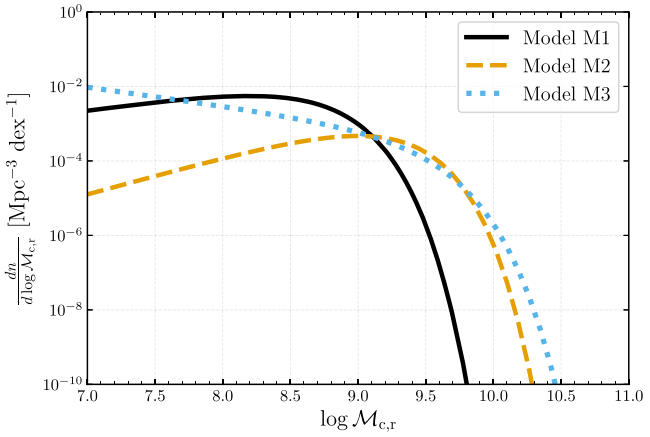



FIG. 2. Comoving SMBHB merger density integrated over redshift of the three population models considered in this work.

the binary mass ratio on $\mathrm{P}(\mathrm{SNR} \geq \mathrm{SNR}_{\mathrm{th}}|\vec{\xi}_{\mathrm{I}})$, we numerically approximate it over a redshift and rest-frame chirp mass grid, fixing $q = 1$. For a given pair of intrinsic parameters, we generate 10000 binaries drawing from uniform distribution their coalescence time $\tau_{\mathrm{c}} \in [\tau_{\mathrm{c}}^{(\mathrm{min})}, 2T^{(\mathrm{max})}]$ and extrinsic parameters; sky location, polarization angle, inclination angle and orbital phase at coalescence. We then compute the SNR of each of these zombie binaries and approximate $\mathrm{P}(\mathrm{SNR} \geq \mathrm{SNR}_{\mathrm{th}}|\vec{\xi}_{\mathrm{I}})$ taking the fraction of binaries satisfying $\mathrm{SNR} \geq \mathrm{SNR}_{\mathrm{th}}$.

To compute the zombies' optimal matched filter SNR, we sum in quadrature the squared SNR contributions from each pulsar of the PTA,

$$\mathrm{SNR} = \sqrt{\sum_{a=1}^{N_{\mathrm{psr}}} \vec{R}_{\mathrm{z}}^{(a)\,\mathrm{T}} \mathbf{C}_a^{-1} \vec{R}_{\mathrm{z}}^{(a)}}, \tag{12}$$

where $\vec{R}_{\mathrm{z}}^{(a)}$ are the timing residuals induced by the zombie binary in pulsar $a$ and $\mathbf{C}_a$ is the noise covariance matrix of pulsar $a$. We emphasize that, to confidently detect a zombie binary, it is not enough to have a high SNR: the signal must also be observed in the data of multiple pulsars.[3] Otherwise, the possibility that the signal arises purely from intrinsic noise cannot be ruled out. Therefore, in the following, we do not consider a zombie binary to be detectable if only a single pulsar contributes to its SNR, even if the latter exceeds the SNR threshold.

We evaluate the noise covariance matrices of pulsars following [54] and using the ENTERPRISE Python software [55]. We incorporate both the radiometer measurement noise [56]—quantified by its root-mean-square error, $\sigma_{\mathrm{MN}}$—and the red noise process associated with the astrophysical GW background. We model the latter using a power-law power spectral density model with a spectral index of 13/3—typical for a population of circular binaries driven by GW emission [52]—and a corresponding characteristic strain amplitude at 1/year of $3 \times 10^{-15}$.

We also include the effect of timing model marginalization (see Ref. [57] and references therein) in each pulsar covariance matrix. In particular, we incorporate the effect of marginalizing on the pulsars' spin frequency and derivative as well as on the pulsars' sky position, which significantly reduces the sensitivity of the array at GW frequencies below its fundamental frequency, $1/T_{\mathrm{obs}}$, and around the 1/year frequency, respectively.

We note that the PTA detection efficiencies that we derive neglect the presence of potential intrinsic red noise components—such as pulsar spin noise or dispersion measure variation noise—and do not take into account the spatially-correlated nature of the GW background noise. However, these assumptions should not have strong impact on our results, since these red noise components typically have a subdominant contribution to PTA sensitivities at the frequencies where zombie binaries are found (see Sec. VI) [57,58]. Instead, the timing measurement precision of the PTA is expected to have a strong impact on the detectability of zombie binaries.

## VI. RESULTS

In order to quantify the capacity of PTAs to probe zombie binaries, we consider representative configurations for past, current and future PTA datasets, which are summarized in Table II. They aim to represent respectively the sensitivity of the European PTA (EPTA) second data release (referred to as DR2new in [59]), the upcoming International PTA (IPTA) third data release (DR3) and a potential future sensitivity of the Square Kilometer Array (SKA) observatory [60]. For the IPTA DR3-like sensitivity, we consider 130 pulsars present in the previously published collaboration datasets, fixing their observing time to 10 years, with an observing cadence of 5 days. For the SKA configuration, we use 124 pulsars of our IPTA-like dataset with declination angle below 45° [61] and added randomly 6 pulsars from [62]. For pulsars whose distances to Earth could not be estimated, we randomly assign them a distance from 0.5 to 2.5 kiloparsecs using uniform weighting.

TABLE II. PTAs configurations considered in this work. The name, observing time, number of pulsars, observing cadence, root-mean-square timing measurement error, and the maximum photon travel time are shown for each array.

| PTA | $T_{\mathrm{obs}}$ [yr] | $N_{\mathrm{psr}}$ | $\Delta t$ [days] | $\sigma_{\mathrm{MN}}$ | $T^{(\mathrm{max})}$ [kyr] |
|---|---|---|---|---|---|
| EPTA | 10 | 25 | 5 | 1 μs | 12.8 |
| IPTA | 10 | 130 | 5 | 1 μs | 12.8 |
| SKA | 10 | 130 | 7 | 50 ns | 20.4 |

[3]We recall that if $\tau_a < \tau_{\mathrm{c}}$ for pulsar $a$, $\vec{R}_{\mathrm{z}}^{(a)} = \vec{0}$, such that pulsar $a$ is not contributing to the zombie SNR.

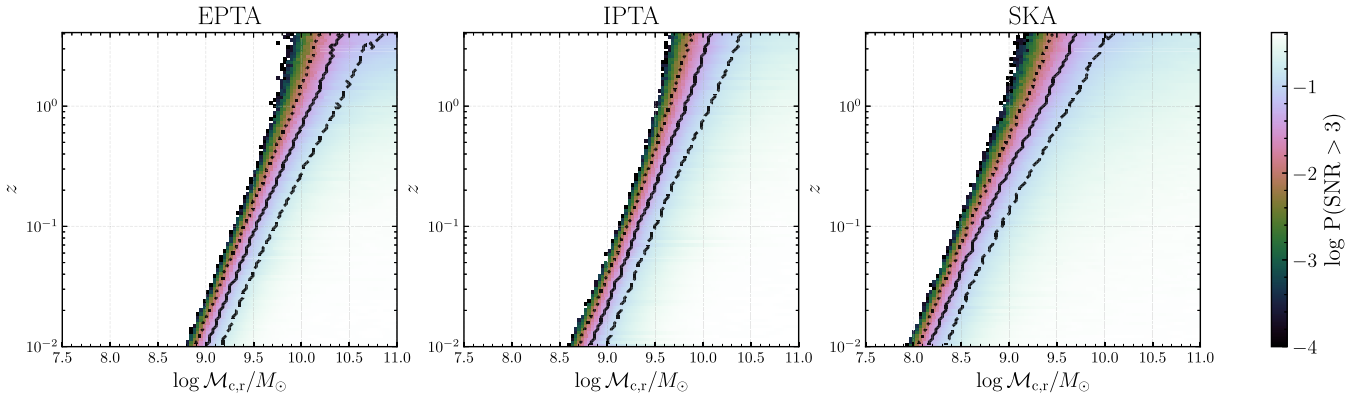



FIG. 3. Detection efficiency for $\mathrm{SNR_{th}} = 3$ of zombie binaries as a function of redshift and rest-frame chirp mass, for the three PTAs configurations considered. See Table II for details on the settings used for each array. Because our estimate of the detection efficiency is based on 10 000 simulated binaries, our sensitivity is restricted to probabilities above $10^{-4}$. We overlay, using dotted, solid, and dashed lines, the contours representing $\mathrm{P(SNR} > \mathrm{SNR_{th}}) \geq 1\%$ with $\mathrm{SNR_{th}} = 3$, 5, and 10, respectively.

In Fig. 3, we show the detection efficiency for zombie binaries, evaluated for each PTA configuration, under the most optimistic detection threshold, $\mathrm{SNR_{th}} = 3$. We find that the EPTA DR2new like dataset can only probe massive systems with $\mathcal{M}_{c,r} \approx 10^9 M_\odot$ at redshift below 0.03. However, such PTAs could probe the very massive—but rare—mergers with $\mathcal{M}_{c,r} \approx 10^{10} M_\odot$ up to $z \approx 1$. Since the SNR of zombie binaries scale as $\sqrt{N_{psr}}$, the situation improves only slightly for our IPTA DR3 setting. However, the true IPTA DR3 dataset will be much more heterogeneous with some pulsars having an observing time longer than 10 years with a better cadence, as well as lower timing precision [14]. This could significantly enhance the detection efficiency of this dataset and we therefore regard our IPTA sensitivity as a conservative baseline. Going to the SKA configuration, we find that zombie binaries of a few billion solar masses (or above) are associated with high detection efficiency up to redshift 1. Less massive mergers with $\mathcal{M}_{c,r} < 10^9 M_\odot$ only have a reasonable chance to exceed the detection threshold providing they happened at very low redshift, typically at $z \lesssim 0.1$.

In order to quantify the dependence of the zombie detection efficiency on the SNR threshold considered, we overlay in Fig. 3 the contours corresponding to $\mathrm{P(SNR} > \mathrm{SNR_{th}}) \geq 1\%$, with $\mathrm{SNR_{th}} = 3$, 5, and 10, shown as dotted, solid, and dashed lines, respectively. At low redshift ($z \lesssim 0.1$), and low chirp masses ($\log \mathcal{M}_{c,r} \lesssim 9.5$), the shifts of the contours toward higher chirp masses simply reflect the scaling of the zombie SNR with the latter.[4] However, at higher redshift and for higher-mass systems, this simple scaling no longer holds. This is due to the red astrophysical GW background noise, which starts to dominate PTAs' sensitivities at low frequency. As opposed to the white measurement noise, this background noise more strongly limits the SNR of zombie binaries as they reach lower orbital frequencies. Consequently, since higher-mass systems evolve more rapidly and thus reach lower pulsar-term GW frequencies, the scaling of the zombie SNR deviates from the low-mass limit. A similar reasoning applies to high-redshift systems, which are also associated with lower redshifted GW frequencies.

Using the numerical detection efficiencies associated with the different SNR thresholds, we then evaluate Eq. (10) for each of the three SMBHBs population models presented in Sec. IV. Our results are summarized in Table III, where we show the probability to have at least one zombie binary with SNR above $\mathrm{SNR_{th}}$ for each PTA-population model pair. While EPTA-like datasets are not likely to be able to detect any zombie binary—$\mathrm{P}(N_z > 0) \leq 3\%$ for all models, with $\mathrm{SNR_{th}} = 3$—the situation strongly improves for IPTA-like and SKA-like datasets. Although the IPTA configuration has a very small chance to have bright zombie binaries in its data under M1—due to its limited detection efficiency for systems with $\mathcal{M}_{c,r} < 10^9 M_\odot$—the probability increases to 23% and 22% for M2 and M3, respectively, considering $\mathrm{SNR_{th}} = 3$. However, these probabilities both drops to 1% under the most conservative threshold, $\mathrm{SNR_{th}} = 10$. Notably, for the SKA-like PTA, $\mathrm{P}(N_z > 0 | \mathrm{SNR_{th}} = 3) \geq 90\%$, for all three population models. We find that such dataset should have, on average, 2.3, 6.1, and 5.7 zombie binaries with SNR larger than 3, considering the M1, M2, and M3 models, respectively. Even in a far more pessimistic scenario where $\sigma_{MN} = 300$ ns for all SKA pulsars, $\langle N_z \rangle$ remains around 1 for both the M2 and M3 models—although it drops to 0.06 for M1. Remarkably, even under the detection threshold $\mathrm{SNR_{th}} = 10$, the occurrence probability remains fairly high for the M2 (51%) and M3 (42%) models. It therefore appears

[4]Indeed, combining Eqs. (1) and (5), it is straightforward to show that the average zombie binary timing residual amplitude scales as $\mathcal{M}_c{}^{15/8}$. Therefore, in Eq. (10), if the noise contribution is assumed to be constant across binaries, we expect, e.g., a factor of $(10/3)^{8/15} \approx 1.9$ between the dotted and dashed contours in Fig. 3, which is indeed recovered.

TABLE III. Occurrence probabilities, $p_{N_z>0}$, and associated expected number of zombie binaries above the detection threshold, $\langle N_z \rangle$, for each population model and SNR detection threshold. We recall that a zombie binary must be observed by at least two pulsars of the array to meet the detection criteria.

| | M1 | | | | | | M2 | | | | | | M3 | | | | | |
|---|---|---|---|---|---|---|---|---|---|---|---|---|---|---|---|---|---|---|
| | SNR > 3 | | SNR > 5 | | SNR > 10 | | SNR > 3 | | SNR > 5 | | SNR > 10 | | SNR > 3 | | SNR > 5 | | SNR > 10 | |
| | $p_{N_z>0}$ | $\langle N_z \rangle$ | $p_{N_z>0}$ | $\langle N_z \rangle$ | $p_{N_z>0}$ | $\langle N_z \rangle$ | $p_{N_z>0}$ | $\langle N_z \rangle$ | $p_{N_z>0}$ | $\langle N_z \rangle$ | $p_{N_z>0}$ | $\langle N_z \rangle$ | $p_{N_z>0}$ | $\langle N_z \rangle$ | $p_{N_z>0}$ | $\langle N_z \rangle$ | $p_{N_z>0}$ | $\langle N_z \rangle$ |
| EPTA | $1.9\times10^{-4}$ | 0.00 | $3.2\times10^{-5}$ | 0.00 | $2.4\times10^{-6}$ | 0.00 | 0.03 | 0.03 | $7.4\times10^{-3}$ | 0.01 | $9.4\times10^{-4}$ | 0.00 | 0.03 | 0.03 | $7.4\times10^{-3}$ | 0.01 | $9.6\times10^{-4}$ | 0.00 |
| IPTA | $2.8\times10^{-3}$ | 0.00 | $5.1\times10^{-4}$ | 0.00 | $4.9\times10^{-5}$ | 0.00 | 0.23 | 0.27 | 0.07 | 0.07 | 0.01 | 0.01 | 0.22 | 0.25 | 0.07 | 0.07 | 0.01 | 0.01 |
| SKA | 0.90 | 2.31 | 0.41 | 0.53 | 0.06 | 0.07 | 1.00 | 6.15 | 0.94 | 2.75 | 0.51 | 0.71 | 1.00 | 5.73 | 0.90 | 2.30 | 0.42 | 0.54 |

likely that, if the spatially-correlated signal observed by the PTA Collaborations truly arises from a population of SMBHBs, the forthcoming SKA dataset will include GW signatures from at least one past binary merger, exhibiting an optimal matched filter SNR in the range [3, 10].

To evaluate the properties of the zombie binaries that the SKA observatory might be able to detect in the future, we sample the distribution, $p(\vec{\xi}_I)$, proportional to the integrand of Eq. (10). Each zombie binary is then assigned a coalescence time and a set of extrinsic parameters; we recall that we assume uniform distributions for the latter. We then select only systems with a SNR higher than 3 for the SKA configuration. We find that the binary population model considered does not significantly impact the distribution of the zombie binaries' parameters. Therefore, in Fig. 4, we only show the distribution obtained using the M3 model.

We find that the bright zombie binaries are massive systems with $\mathcal{M}_{c,r} > 10^9 M_\odot$, located at low redshift; 95% of them are found at $z < 1.5$, under M3. These high masses are required in order to have a significant frequency evolution in the thousands of years separating the pulsar terms' epochs from the binary coalescence. Despite the *a priori* uniform distribution on $\tau_c$, we find that the bright zombie binaries are typically merging close to the PTA starting date; less than 5% of these systems merge more than 8.4 thousand years before $t_0$. This behavior is expected; as shown in the corresponding cells of Fig. 4, the smaller $\tau_c$ is, the more pulsars can observe the binary before its merger, and thus the higher its SNR becomes. As a result, as illustrated in the $N_{psr}$ column of Fig. 4, the number of pulsars contributing to the SNR of zombie binaries generally reaches several dozen for the SKA configuration. This could allow their identification through the sky-dependent frequency signature of their pulsar terms; a distinctive feature of these systems. In the Appendix, we quantify more precisely the number of contributing pulsars by determining how many are required to achieve 90% of the $SNR^2$ threshold.

Finally, since the coalescence of these binaries of a few billion solar masses typically occurs thousands of years after the pulsar terms' epochs, we expect the GW frequencies associated to the latter to be found around 10–20 nanohertz (as predicted in Fig. 1). This is confirmed in Fig. 4, which displays the distribution of the mean GW frequency, $\langle f_{GW}^{(P)} \rangle$, associated with the pulsar terms of the zombie binaries. To obtain this mean frequency for a given system, we consider only those pulsars whose pulsar terms are sensitive to the binary inspiral and thus contribute to the SNR calculation. We find, under M3, that 90% of the bright zombie binaries verify $\log\langle f_{GW}^{(P)} \rangle \in [-8.2, -7.5]$.[5] Incidentally, this represents an optimal range that lies between the reduced sensitivity of PTAs at higher frequencies (mainly caused by the timing precision, observing cadence and the response of timing residuals to GWs) and the low-frequency regime where red noise dominates (arising from both the GW background(s) and intrinsic red noise processes). This frequency range where bright zombie binaries are most likely found could thus mitigate false alarm detections caused by particular red noise realizations. A dedicated detectability analysis based on simulated PTA datasets is required to investigate this hypothesis further.

## VII. DISCUSSION

In this work, we demonstrated that PTAs have the capacity of probing the mergers of SMBHBs that occurred before the start of the experiment. This new class of PTA sources—which we call zombie binaries—are accessible thanks to the time delays of several thousands of years that separate the so-called pulsar term from the Earth term in the timing residuals induced by a GW source.

Considering the case of circular binaries driven by GW emission, we estimated the number of zombie binaries with a SNR greater than 3 that past (EPTA DR2), current (IPTA DR3) and future (SKA) PTA datasets are likely to be sensitive to. In order to capture the current uncertainty on the merger rate of SMBHBs, we considered three analytic

[5]We note that under the M1 population model, which admits a lower chirp mass cutoff, this interval shifts towards higher frequencies, $\log\langle f_{GW}^{(P)} \rangle \in [-7.85, -7.34]$, due to the slower dynamical evolution of lower-mass systems.

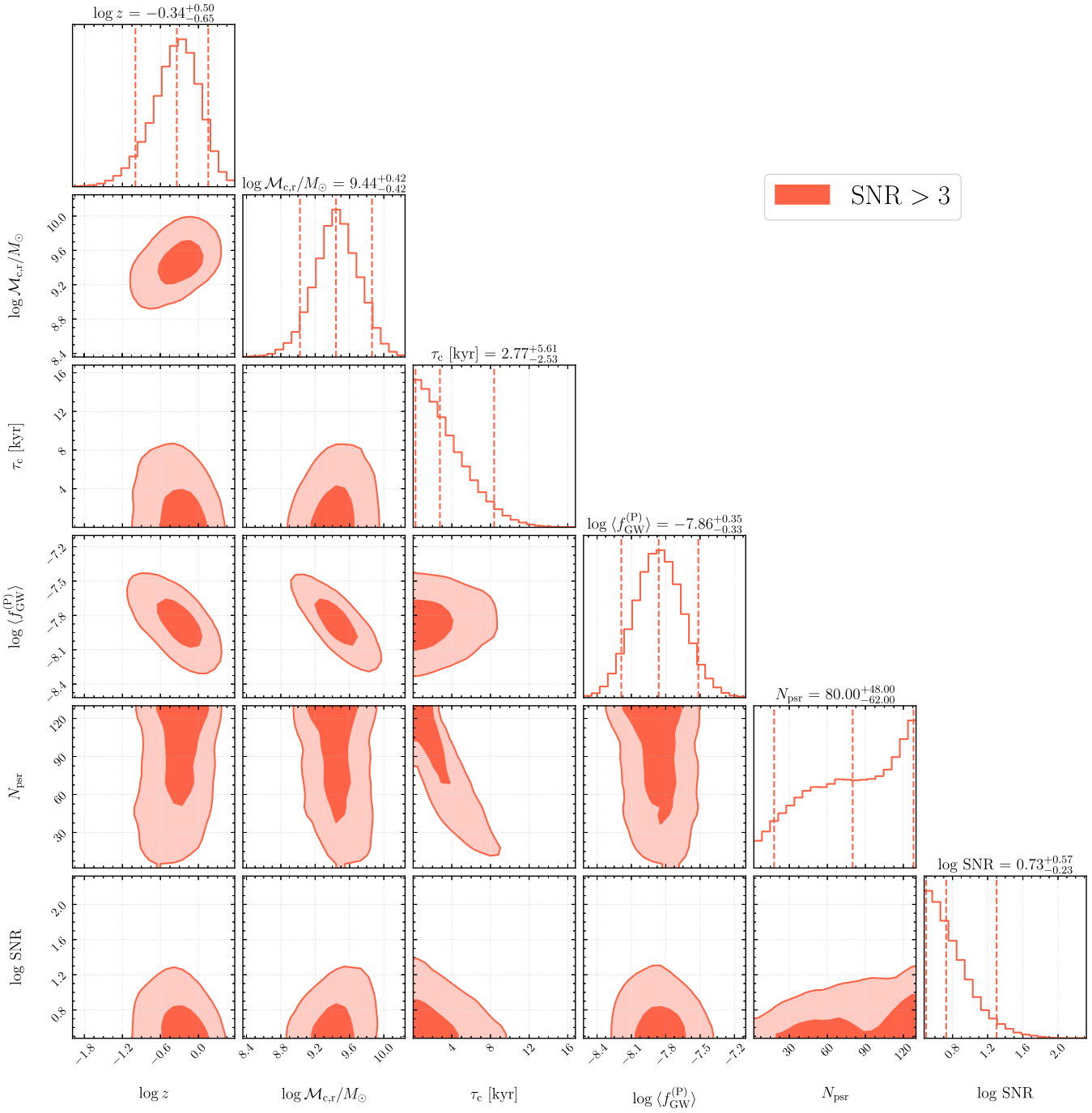



FIG. 4. 2D distribution of the properties of zombie binaries with a SNR greater than 3 in the SKA configuration, assuming the M3 population model. In addition to the intrinsic properties of the merger, we report the number of pulsars $N_{\rm psr}$ that actually observe the binary before its coalescence—and therefore contribute to its potential detection—and the average GW frequency of their pulsar terms, $\langle f_{\rm GW}^{(\rm P)} \rangle$.

comoving merger density models—based on Schechter-like functions—compatible with current PTA observations. While EPTA DR2-like datasets lack sensitivity to yield a significant probability of detecting zombie binaries, we find that, for SMBHBs models favoring large mass systems (with $\mathcal{M}_{\rm c,r} > 10^9 M_\odot$), the IPTA DR3 dataset has a 23% probability of containing at least one zombie binary with SNR $> 3$. For the SKA sensitivity considered here, we find that, for all population models, this probability is greater than 90%. We predict that a few bright zombie binaries—with SNR in the range [3, 10]—are likely to be present in future SKA datasets if the currently observed PTA signal is sourced by a population of SMBHBs. These massive mergers ($\mathcal{M}_{\rm c,r} > 10^9 M_\odot$) associated with pulsar term

signals' frequency on the order of 10 nanohertz, will typically be probed at low redshift ($z \lesssim 1$). However, we note that these findings rely on the assumption that SMBHBs are on circular orbits. If the signal observed by PTAs originates from a population of binaries that are on very eccentric orbits when entering the PTA band—as recent studies suggest [63,64]—then zombie binaries may still have significant eccentricities. Because the orbital evolution of eccentric binaries is faster, zombie binaries could be found at lower orbital frequencies than in the circular case. This should be explored in future work.

We also note that the SNR calculations used in this work do not account for our current uncertainty about the pulsar distances and therefore could be considered optimistic. However, precise distance measurements using very long baseline interferometry are becoming increasingly common for millisecond pulsars [65]. In addition, the significant improvement in timing precision allowed by the SKA is expected to enable pulsar distance measurements with less than 5% error for the pulsars' distances considered in this work [66]. Achieving a distance accuracy for pulsars on the order of hundreds of light-years will allow precise determination of the frequencies of the pulsar terms. This will help the coherent reconstruction of zombie binary signals across multiple pulsars, which is required for a future robust detection.

It is also important to recall that the optimal matched filter SNR considered in this work does not capture the complexity of realistic pulsar noise models, which include intrinsic noise components along with different potential common correlated signals. In addition, the SKA will most likely be capable of detecting individual SMBHBs [27,67] whose signals could partially overlap with those of zombie binaries. Although the latter only significantly affect a subset of pulsars and yield different GW frequencies in each pulsar of the array, the simultaneous search for standard continuous wave signals from SMBHBs could also affect the detectability of zombie binaries. The assessment of zombie binaries' detectability in realistic simulated PTA datasets is deferred to future work.

Such indirect detection of past binary mergers would open a remarkable window on the study of the environment and dynamics of SMBHBs during the last thousands of years before coalescence. However, it will also represent a challenge for detecting their signals, since the waveform associated with each pulsar of the array depends on the orbital frequency evolution model considered. In any case, the search for zombie binaries will—and could already—put new constraints on the high-mass end of SMBHBs merger rate models.

*Softwares*: Astropy [68], CORNER [69], JAX [70], NumPy [71], SciPy [72].

## ACKNOWLEDGMENTS

This work was supported by the European Union's H2020 ERC Advanced Grant "PINGU" (Grant Agreement No. 101142079). H. Q. L. is grateful to A. Sesana for helpful discussions. H. Q. L. also thanks A. Sesana, S. Babak, and M. Falxa for their comments on this manuscript. H. Q. L. thanks the anonymous referee for constructive comments that greatly improved the manuscript. Numerical computations were partly performed on the CC-IN2P3 (CNRS), in France.

## DATA AVAILABILITY

The data and scripts used to produce the findings of this work are openly available at [73].

## APPENDIX: NUMBER OF CONTRIBUTING PULSARS TO THE ZOMBIE SNRs

In this section, we aim to determine how many pulsars typically make a significant contribution to the total SNR of bright zombie binaries. To this end, we use the bright

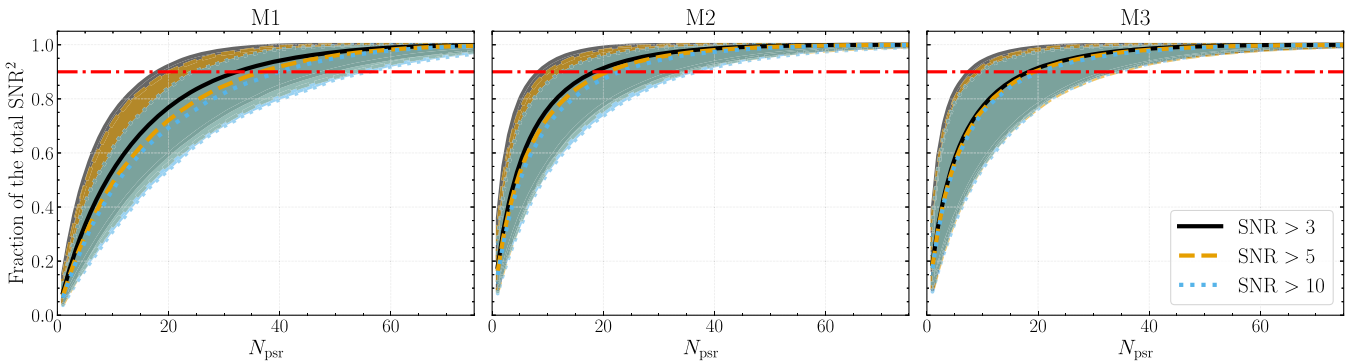



FIG. 5. Distribution of the cumulative fraction of the total $SNR^2$ for bright zombie binaries—as seen by the SKA configuration—shown for different population models and various total SNR range. Note that we limit the visualization to $N_{psr} \leq 75$, although the SKA configuration includes 130 pulsars. The medians and corresponding 68% confidence intervals are represented by lines and shaded regions, respectively. For the M2 and M3 models—displayed in the middle and right panels, respectively—we find that, for half of the bright systems, the contributions from roughly 20 pulsars must be combined to recover at least 90% of the total $SNR^2$ of the source.

zombie binary samples associated with the different population models, as shown in Fig. 4 for M3. For each system, we calculate the individual optimal matched filter $SNR^2$ for every pulsar in the array. We then sort these individual contributions in descending order and evaluate the fraction of the total squared SNR as a function of the number of pulsar contributions included. Combining these contributions from each bright zombie binary, we estimate the distribution of this cumulative $SNR^2$ fraction function. The results are shown for the SKA configuration in Fig. 5, where we display both the median and the 68% confidence intervals of the obtained distributions. The M2 and M3 models yield very similar results. In most cases, the number of pulsars required to reach 90% of the total squared SNR ranges from 6 to 35, with an almost negligible dependence on the total SNR of the source. Conversely, bright zombie binaries in the M1 model require a larger number of pulsar contributions to attain such a fraction of the total signal power. This is due to the fact that bright zombie binaries in M1 have lower chirp masses than the bright systems found in M2 and M3, and therefore undergo a slower dynamical evolution. Consequently, the GW frequencies of their associated pulsar terms are higher and therefore yield smaller timing residual amplitudes. These binaries thus need to be observed by a larger number of pulsars in order to reach a significant squared SNR.


[1] J. Antoniadis *et al.*, The second data release from the European Pulsar Timing Array. III. Search for gravitational wave signals, Astron. Astrophys. **678**, A50 (2023).

[2] G. Agazie *et al.*, The NANOGrav 15 yr data set: Evidence for a gravitational-wave background, Astrophys. J. Lett. **951**, L8 (2023).

[3] H. Xu *et al.*, Searching for the nano-hertz stochastic gravitational wave background with the Chinese Pulsar Timing Array data release I, Res. Astron. Astrophys. **23**, 075024 (2023).

[4] D. J. Reardon *et al.*, Search for an isotropic gravitational-wave background with the Parkes Pulsar Timing Array, Astrophys. J. Lett. **951**, L6 (2023).

[5] M. T. Miles *et al.*, The MeerKAT Pulsar Timing Array: The first search for gravitational waves with the MeerKAT radio telescope, Mon. Not. R. Astron. Soc. **536**, 1489 (2025).

[6] M. Rajagopal and R. W. Romani, Ultra–low-frequency gravitational radiation from massive black hole binaries, Astrophys. J. **446**, 543 (1995).

[7] A. H. Jaffe and D. C. Backer, Gravitational waves probe the coalescence rate of massive black hole binaries, Astrophys. J. **583**, 616 (2003).

[8] J. P. Ostriker and M. A. Hausman, Cannibalism among the galaxies: Dynamically produced evolution of cluster luminosity functions, Astrophys. J. **217**, L125 (1977).

[9] C. Lacey and S. Cole, Merger rates in hierarchical models of galaxy formation, Mon. Not. R. Astron. Soc. **262**, 627 (1993).

[10] M. Milosavljević and D. Merritt, Long-term evolution of massive black hole binaries, Astrophys. J. **596**, 860 (2003).

[11] M. C. Begelman, R. D. Blandford, and M. J. Rees, Massive black hole binaries in active galactic nuclei, Nature (London) **287**, 307 (1980).

[12] G. D. Quinlan, The dynamical evolution of massive black hole binaries I. Hardening in a fixed stellar background, New Astron. **1**, 35 (1996).

[13] R. W. Hellings and G. S. Downs, Upper limits on the isotropic gravitational radiation background from pulsar timing analysis., Astrophys. J. Lett. **265**, L39 (1983).

[14] G. Agazie *et al.*, Comparing recent Pulsar Timing Array results on the nanohertz stochastic gravitational-wave background, Astrophys. J. **966**, 105 (2024).

[15] A. Afzal *et al.*, The NANOGrav 15 yr data set: Search for signals from new physics, Astrophys. J. Lett. **951**, L11 (2023).

[16] J. Antoniadis *et al.*, The second data release from the European Pulsar Timing Array. IV. Implications for massive black holes, dark matter, and the early Universe, Astron. Astrophys. **685**, A94 (2024).

[17] C. M. F. Mingarelli, T. Sidery, I. Mandel, and A. Vecchio, Characterizing gravitational wave stochastic background anisotropy with pulsar timing arrays, Phys. Rev. D **88**, 062005 (2013).

[18] N. M. Jiménez Cruz, A. Malhotra, G. Tasinato, and I. Zavala, Measuring kinematic anisotropies with pulsar timing arrays, Phys. Rev. D **110**, 063526 (2024).

[19] M. Falxa, H. Quelquejay Leclere, and A. Sesana, From eccentric binaries to nonstationary gravitational wave backgrounds, Phys. Rev. D **111**, 023047 (2025).

[20] W. G. Lamb, J. M. Wachter, A. Mitridate, S. C. Sardesai, B. Bécsy, E. L. Hagen, S. R. Taylor, and L. Z. Kelley, Finite populations & finite time: The non-Gaussianity of a gravitational wave background, Phys. Rev. D **113**, 123065 (2026).

[21] M. Falxa and A. Sesana, Modeling non-Gaussianities in pulsar timing array data analysis using Gaussian mixture models, Phys. Rev. D **113**, 043047 (2026).

[22] M. Falxa *et al.*, Modeling nonstationary noise in pulsar timing array data analysis, Phys. Rev. D **109**, 123010 (2024).

[23] K. Grunthal *et al.*, The MeerKAT Pulsar Timing Array: Maps of the gravitational wave sky with the 4.5-yr data release, Mon. Not. R. Astron. Soc. **536**, 1501 (2025).

[24] G. Agazie *et al.*, The NANOGrav 15 yr data set: Search for anisotropy in the gravitational-wave background, Astrophys. J. Lett. **956**, L3 (2023).

[25] Y. Chen *et al.*, Searching for anisotropy in the gravitational wave background using the Parkes Pulsar Timing Array, Phys. Rev. D **113**, 043042 (2026).

[26] A. N. Lommen and D. C. Backer, Using pulsars to detect massive black hole binaries via gravitational radiation: Sagittarius A* and nearby galaxies, Astrophys. J. **562**, 297 (2001).
[27] A. Sesana, A. Vecchio, and M. Volonteri, Gravitational waves from resolvable massive black hole binary systems and observations with pulsar timing arrays, Mon. Not. R. Astron. Soc. **394**, 2255 (2009).
[28] S. R. Taylor, E. A. Huerta, J. R. Gair, and S. T. McWilliams, Detecting eccentric supermassive black hole binaries with pulsar timing arrays: Resolvable source strategies, Astrophys. J. **817**, 70 (2016).
[29] G. Agazie *et al.*, The NANOGrav 15 yr data set: Bayesian limits on gravitational waves from individual supermassive black hole binaries, Astrophys. J. Lett. **951**, L50 (2023).
[30] J. Antoniadis *et al.*, The second data release from the European Pulsar Timing Array. V. Search for continuous gravitational wave signals, Astron. Astrophys. **690**, A118 (2024).
[31] L. S. Finn and A. N. Lommen, Detection, localization, and characterization of gravitational wave bursts in a pulsar timing array, Astrophys. J. **718**, 1400 (2010).
[32] R. van Haasteren and Y. Levin, Gravitational-wave memory and pulsar timing arrays, Mon. Not. R. Astron. Soc. **401**, 2372 (2010).
[33] D. R. Madison, J. M. Cordes, and S. Chatterjee, Assessing pulsar timing array sensitivity to gravitational wave bursts with memory, Astrophys. J. **788**, 141 (2014).
[34] J. M. Cordes and F. A. Jenet, Detecting gravitational wave memory with pulsar timing, Astrophys. J. **752**, 54 (2012).
[35] J. B. Wang *et al.*, Searching for gravitational wave memory bursts with the Parkes Pulsar Timing Array, Mon. Not. R. Astron. Soc. **446**, 1657 (2015).
[36] S. M. Tomson, B. Goncharov, R. van Haasteren, R. Srinivasan, E. Barausse, Y. Wen, J. Wang *et al.*, Search for gravitational-wave memory in PPTA and EPTA data: A complete signal model, Astrophys. J. Lett. **996**, L9 (2026).
[37] M. Pitkin, J. Clark, M. A. Hendry, I. S. Heng, C. Messenger, J. Toher, and G. Woan, Is there potential complementarity between LISA and pulsar timing?, J. Phys. Conf. Ser. **122**, 012004 (2008).
[38] A. D. A. M. Spallicci, On the complementarity of pulsar timing and space laser interferometry for the individual detection of supermassive black hole binaries, Astrophys. J. **764**, 187 (2013).
[39] S. Detweiler, Pulsar timing measurements and the search for gravitational waves, Astrophys. J. **234**, 1100 (1979).
[40] A. Sesana and A. Vecchio, Measuring the parameters of massive black hole binary systems with pulsar timing array observations of gravitational waves, Phys. Rev. D **81**, 104008 (2010).
[41] P. C. Peters, Gravitational radiation and the motion of two point masses, Phys. Rev. **136**, 1224 (1964).
[42] P. C. Peters and J. Mathews, Gravitational radiation from point masses in a Keplerian Orbit, Phys. Rev. **131**, 435 (1963).
[43] M. Enoki, K. T. Inoue, M. Nagashima, and N. Sugiyama, Gravitational waves from supermassive black hole coalescence in a hierarchical galaxy formation model, Astrophys. J. **615**, 19 (2004).
[44] A. Sesana, A. Vecchio, and C. N. Colacino, The stochastic gravitational-wave background from massive black hole binary systems: Implications for observations with Pulsar Timing Arrays, Mon. Not. R. Astron. Soc. **390**, 192 (2008).
[45] S. Chen, A. Sesana, and C. J. Conselice, Constraining astrophysical observables of galaxy and supermassive black hole binary mergers using pulsar timing arrays, Mon. Not. R. Astron. Soc. **488**, 401 (2019).
[46] Planck Collaboration *et al.*, Planck 2018 results. VI. Cosmological parameters, Astron. Astrophys. **641**, A6 (2020).
[47] D. W. Hogg, Distance measures in cosmology, arXiv:astro-ph/9905116.
[48] S. Kay, *Fundamentals of Statistical Signal Processing: Detection theory*, Fundamentals of Statistical Signal Processing (Prentice-Hall, Prentice, NJ, 1998).
[49] D. Daley and D. Vere-Jones, *An Introduction to the Theory of Point Processes*, Springer Series in Statistics (Springer, New York, 2013).
[50] H. Middleton, W. Del Pozzo, W. M. Farr, A. Sesana, and A. Vecchio, Astrophysical constraints on massive black hole binary evolution from pulsar timing arrays, Mon. Not. R. Astron. Soc. **455**, L72 (2016).
[51] G. Sato-Polito and M. Kamionkowski, Exploring the spectrum of stochastic gravitational-wave anisotropies with pulsar timing arrays, Phys. Rev. D **109**, 123544 (2024).
[52] E. S. Phinney, A practical theorem on gravitational wave backgrounds, arXiv:astro-ph/0108028.
[53] G. Agazie *et al.*, The NANOGrav 15 yr data set: Constraints on supermassive black hole binaries from the gravitational-wave background, Astrophys. J. Lett. **952**, L37 (2023).
[54] R. van Haasteren and M. Vallisneri, New advances in the Gaussian-process approach to pulsar-timing data analysis, Phys. Rev. D **90**, 104012 (2014).
[55] J. A. Ellis, M. Vallisneri, S. R. Taylor, and P. T. Baker, ENTERPRISE: Enhanced Numerical Toolbox Enabling a Robust PulsaR Inference SuitE, Zenodo, 10.5281/zenodo.4059815 (2020).
[56] J. P. W. Verbiest and G. M. Shaifullah, Measurement uncertainty in pulsar timing array experiments, Classical Quantum Gravity **35**, 133001 (2018).
[57] J. S. Hazboun, J. D. Romano, and T. L. Smith, Realistic sensitivity curves for pulsar timing arrays, Phys. Rev. D **100**, 104028 (2019).
[58] C. J. Moore, S. R. Taylor, and J. R. Gair, Estimating the sensitivity of pulsar timing arrays, Classical Quantum Gravity **32**, 055004 (2015).
[59] J. Antoniadis *et al.*, The second data release from the European Pulsar Timing Array. I. The dataset and timing analysis, Astron. Astrophys. **678**, A48 (2023).
[60] R. M. Shannon *et al.*, The SKAO Pulsar Timing Array, Open J. Astrophys. **8**, 54243 (2025).
[61] G. Janssen *et al.*, Gravitational wave astronomy with the SKA, Proc. Sci. AASKA14 (**2015**) 037.
[62] S. Chatterjee, https://hosting.astro.cornell.edu/research/parallax/, version used: March, 2025.
[63] J. Raidal, J. Urrutia, V. Vaskonen, and H. Veermäe, Eccentricity effects on the supermassive black hole gravitational wave background, Astron. Astrophys. **691**, A212 (2024).

[64] F. Fastidio, E. Bortolas, A. Gualandris, A. Sesana, J. I. Read, and W. Dehnen, Realistic consecutive galaxy mergers form eccentric pulsar timing array sources, Astron. Astrophys. **703**, A86 (2025).
[65] A. T. Deller *et al.*, Microarcsecond VLBI pulsar astrometry with PSR$\pi$ II. Parallax distances for 57 pulsars, Astrophys. J. **875**, 100 (2019).
[66] R. Smits, S. J. Tingay, N. Wex, M. Kramer, and B. Stappers, Prospects for accurate distance measurements of pulsars with the square kilometre array: Enabling fundamental physics, Astron. Astrophys. **528**, A108 (2011).
[67] R. J. Truant, D. Izquierdo-Villalba, A. Sesana, G. Mohiuddin Shaifullah, M. Bonetti, D. Spinoso, and S. Bonoli, Lighting up the nanohertz gravitational wave sky: Opportunities and challenges of multimessenger astronomy with pulsar timing array experiments, Astron. Astrophys. **706**, A115 (2026).
[68] Astropy Collaboration, The Astropy project: Sustaining and growing a community-oriented open-source project and the latest major release (v5.0) of the CoRe package, Astrophys. J. **935**, 167 (2022).
[69] D. Foreman-Mackey, CORNER.PY: Scatterplot matrices in Python, J. Open Source Software **1**, 24 (2016).
[70] J. Bradbury *et al.*, JAX: Composable transformations of Python + NumPy programs (2018), https://github.com/jax-ml/jax/blob/main/CITATION.bib.
[71] C. R. Harris *et al.*, Array programming with NumPy, Nature (London) **585**, 357 (2020).
[72] P. Virtanen *et al.*, SciPy 1.0: Fundamental algorithms for scientific computing in Python, Nat. Methods **17**, 261 (2020).
[73] https://github.com/hquelquejay/zombie-binaries-pta.